Optical Measurements of Surface Plasmons in Gold

A. S. Barker, Jr.
Bell Laboratories, Murray Hill, New Jersey 07974
(Received 13 July 1973)

The absorption associated with surface plasmons at a gold-air interface is measured using an evanescent wave coupler. The measurements cover the energy range 1.8–3 eV. Scans made for different values of surface wave vector in the range 1.2×10^5–2.7×10^5 cm^{-1} give the dispersion of the surface plasmon both for the gold-air interface and for a gold-silica interface, and also yield the optical constants of gold. Good agreement is obtained with lower-energy measurements of the dispersion by Ritchie *et al*. An analysis of the range of surface plasmons is presented using the present data and the Drude approximation for extrapolation into the infrared where the range increases to several centimeters.

I. INTRODUCTION

The concept of bulk or volume plasmons in metals has been well established, both theoretically and experimentally. These longitudinal polarization fluctuations obey the resonance condition $\epsilon = 0$, where ϵ is the dielectric function of the metal.[1] Over the past fifteen years it has become evident that there is an additional plasmonlike mode associated with surfaces and interfaces. In a theoretical paper, Ritchie discovered loss peaks for energetic electrons passing through foils not only at the volume plasmon frequency but also at a lower energy.[2] He called these latter loss peaks "lowered" plasmon modes and noted their connection with the foil boundaries. Stern and Farrell derived the resonance condition for these modes and called them surface plasmons.[3] They used a dielectric function approach to the free-electron gas and obtained the resonance condition $\epsilon = -\epsilon_0$, where ϵ_0 is the dielectric function of the medium contiguous with the metal surface. For a metal-air surface their result is

$$\epsilon = -1 , \tag{1}$$

for the surface-plasmon resonance condition. The surface-plasmon modes have been detected by fast-electron scattering in metallic foils with and without oxide overlays by Kunz.[4] There is good agreement with Eq. (1) once dispersion is taken into account. Equation (1) turns out to be the resonance condition for surface plasmons whose wave vector $k_{\parallel}$ is much less than the Fermi-Thomas wave vector but much greater than ω/c, where ω is the frequency of the mode and c the velocity of light.

More recently, Otto discovered a method of coupling an optical beam to surface plasmons.[5] This method uses a coupling prism adjacent to the metal surface and depends on the evanescent field of the optical beam penetrating a small distance into the metal to couple with the polarization field of the surface plasmon. This method of coupling has been called the attenuated-total-reflection (ATR) method.[6] Unlike the fast-electron-scattering method, it allows very precise measurement of the frequency and wave vector of the surface plasmons. Otto was able to investigate the surface plasmon in silver and check its dispersion in the retardation region where $k_{\parallel} \sim \omega/c$. Very recently, the method has been extended to surface excitations of phonon[7–9] and free-carrier[8] character in insulators and semiconductors. Equation (1) is still the resonance condition, though the polarization field in the medium is now made up of charged-ion motion in the phonon case rather than free-electron motion as in the metallic case.

Figure 1 shows the standard geometry for discussion of surface excitations. A sharp boundary at $z = 0$ separates two media. We take the top medium to be air with $\epsilon = 1$. Figure 1(b) shows the

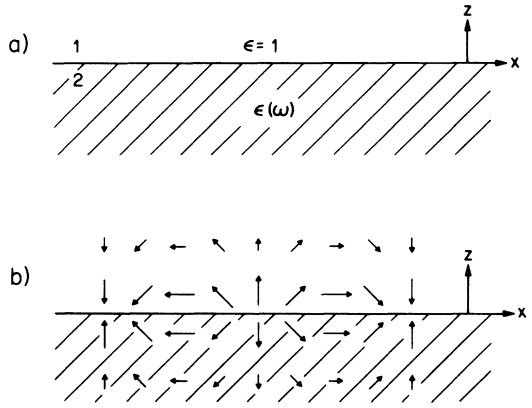

FIG. 1. (a) Flat interface between two media of dielectric constant $\epsilon = 1$ and $\epsilon(\omega)$. The z axis is chosen as the outward normal to the medium of interest. (b) Electric field pattern for a surface polariton. The fields die off exponentially away from $z = 0$ but rotate along x. The pattern has been drawn for a large-wave-vector excitation. The accompanying magnetic fields are normal to the paper.

electric field pattern for a surface plasmon. The amplitude falls off exponentially as $e^{-q_1 z}$ in medium 1 and as $e^{q_2 z}$ in medium 2. A true surface excitation must have $\mathrm{Re}q_1$ and $\mathrm{Re}q_2$ both positive. In earlier papers[8,10] the present author developed the response function, or impedance T, for the surface mode to an externally applied surface charge σ_{ext}. Table I gives the result for T for an air-medium interface. Since natural surface modes occur at the poles of T, we find Eq. (1) directly from the table in the large-$k_{\parallel}$ approximation. The resonance condition for arbitrary $k_{\parallel}$ is also given in the table. Since the techniques of this paper measure the surface-mode frequency and line shape, we can go beyond the specification of a resonance condition. The analysis carried out below can give the response function T in detail [and hence $\epsilon(\omega)$] rather than just the resonances (poles) of T.

The present paper presents results for the surface plasmons in gold. The coupler prism method is used to examine the surface-plasmon frequency and line shape. In addition, the dispersion of the surface-plasmon frequency ω as a function of $k_{\parallel}$ in the retardation region is measured. The present dispersion curve extends the region studied earlier by Ritchie *et al.* using a different method.[11] In the process of fitting the data, the optical constants of gold are evaluated from the surface-plasmon absorption and found to be very close to the bulk optical constants measured by more conventional techniques. In Sec. II the necessary experimental details are given together with the equations needed to analyze the ATR data. Section III presents the results for the optical constants of gold together with the data fits which determine them. In Sec. IV the results for the surface-plasmon dispersion are presented and some calculations of the propagation range of the plasmons discussed. The necessary equations for the range evaluation are given in an appendix.

II. EXPERIMENTAL

Figure 2 shows the geometry used in measuring the surface-phasmon spectra using a coupler prism. Light of frequency ω and wavelength $\lambda = 2\pi c/\omega$ is directed into a prism whose index is n_0. The angle of incidence at the bottom interface inside the prism is θ_0. For most of the experiments described below θ_0 ranged from 46° to 75°. The beam was collimated to the extent that it contained rays which deviated at most 1.5° from the nominal direction inside the prism. The condition $n_0 \sin\theta_0 > 1$ was always maintained so that in the absence of a sample the field below the coupling prism had evanescent form as shown in Fig. 2(a). For a p-polarized incident beam the electric field has the distribution shown with spatial repeat distance l. The corresponding wave vector is

$$k_{\parallel} = n_0 \omega (\sin\theta_0)/c ; \tag{2}$$

surface plasmons of this wave vector can be excited and observed by monitoring the reflected power[5,8] at D in Fig. 2(b).

The evanescent field shown in Fig. 2(a) decreases exponentially in the $-z$ direction according to

$$|E| \propto \exp[z\omega(n_0^2 \sin^2\theta_0 - 1)^{1/2}/c] . \tag{3}$$

From Eq. (3) we see that for $n_0 \sin\theta_0 \gg 1$ the characteristic distance of penetration of the field below the coupling prism is

$$d \approx \lambda/(2\pi n_0 \sin\theta_0) . \tag{4}$$

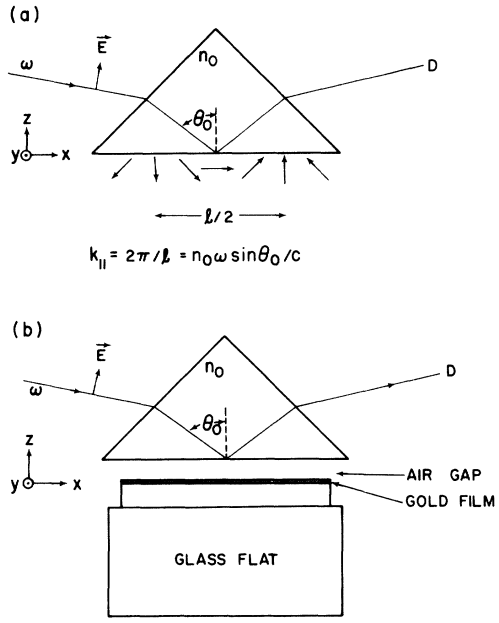

FIG. 2. (a) Light beam directed into a coupling prism so that only an evanescent field exists below the prism. The evanescent field is sketched in and its wave vector defined. (b) The coupling prism is brought close to a gold sample so that the evanescent field can probe the gold surface.

TABLE I. Electric field response function for an air-dielectric interface to applied surface-charge wave of the form $\sigma_{ext} \propto \exp[i(k_{\parallel}x - \omega t)]$.

$T \equiv E_2^{\perp}(z=0)/4\pi\sigma_{ext}$	
$\omega \ll ck_{\parallel}$ (no retardation)	Retardation included
$T = \dfrac{1}{-\epsilon - 1}$	$T = \left[-\epsilon - \left(\dfrac{1-\epsilon\omega^2/c^2k_{\parallel}^2}{1-\omega^2/c^2k_{\parallel}^2}\right)^{1/2}\right]^{-1}$
$q_1 = k_{\parallel}$	$q_1 = (k_{\parallel}^2 - \omega^2/c^2)^{1/2}$
$q_2 = k_{\parallel}$	$q_2 = (k_{\parallel}^2 - \epsilon\omega^2/c^2)^{1/2}$

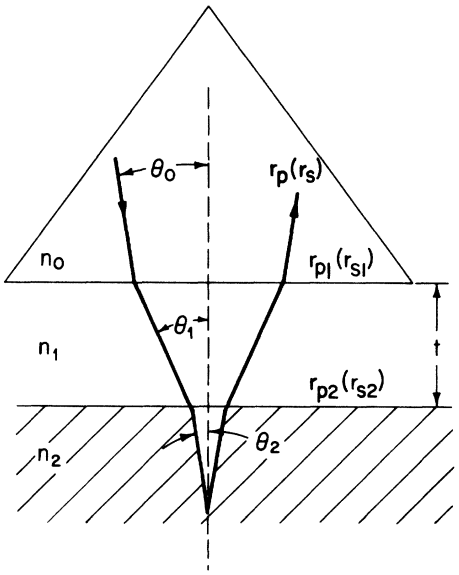

FIG. 3. Detailed layout of the three media involved in the prism coupler technique. Note that angles θ_1 and θ_2 will be complex in Snell's law when the coupler is used correctly. The over-all amplitude reflectivity is r_p where r_{p1} and r_{p2} are the individual interface reflectivities for p-polarized light. The corresponding quantities for s-polarized light are shown in parentheses.

As Eq. (4) shows, air-gap spacings of a few hundredths of a micron are needed for the present experiments in the visible region of the spectrum.

In the simplest case of an isotropic prism, air gap and isotropic metal (gold) surface as shown in Fig. 2, the equation which gives the reflectivity *inside the prism* is

$$r_p = \frac{r_{p1} + r_{p2} e^{-2i\delta_1}}{1 + r_{p1} r_{p2} e^{-2i\delta_1}} , \tag{5}$$

where r_p is the amplitude reflectivity for p-polarized light in medium 0 and r_{p1} and r_{p2} are the individual interface reflectivities at the media 0, 1 and 1, 2 interfaces (see Fig. 3). The notation is taken from Heaven's book.[12] r_{p1} is given by

$$r_{p1} = \frac{n_0 \cos\theta_1 - n_1 \cos\theta_0}{n_0 \cos\theta_1 + n_1 \cos\theta_0} , \tag{6}$$

with a similar equation for r_{p2} involving the refractive indices n_1 and n_2 and the angles θ_1 and θ_2. The angle is given by the experimental arrangement. The two angles θ_1 and θ_2 are obtained from Snell's law:

$$n_0 \sin\theta_0 = n_1 \sin\theta_1 = n_2 \sin\theta_2. \tag{7}$$

Note that θ_1 and θ_2 may be complex. The remaining parameter δ, which expresses the phase, is given by

$$\delta_1 = (2\pi n_1 t \cos\theta_1)/\lambda. \tag{8}$$

The measured power reflectivity R_p, when corrected for any losses with entering and leaving medium 0 (the prism), is given by

$$R_p = |r_p|^2. \tag{9}$$

Figure 3 shows the principal quantities involved. As discussed below, most of the experiments involved measuring R_p/R_s. R_s is obtained in a similar manner; the principal difference is the change of Eq. (6) to the form

$$r_{s1} = \frac{n_0 \cos\theta_0 - n_1 \cos\theta_1}{n_0 \cos\theta_0 + n_1 \cos\theta_1} , \tag{10}$$

with a similar form for r_{s2} involving subscript changes $0 \to 1$, $1 \to 2$. Equation (9) and the corresponding equations for R_p have been calculated for a range of wavelengths using the square root of the dielectric function of gold for n_2.

Gold samples were prepared by evaporation of gold (99.999% purity) approximately 2000 Å thick onto cleaned microscope slides. The substrate was held at 300 K and the evaporation proceeded at 100 Å/sec. The slide was then backed up with a $\frac{1}{2}$-in. -thick glass flat and assembled against the prism as shown in Fig. 2. For some runs, aluminum dots were evaporated on top of the gold as spacers to control the air-gap thickness. For many of the runs natural dust particles provided the spacers and the beam was moved around inside the prism to obtain a region of suitable air gap. In many cases the gap could be estimated by observing Newton's rings in the air-gap region.

All measurements were made with a single-beam prism spectrometer. Figure 4 shows the coupler

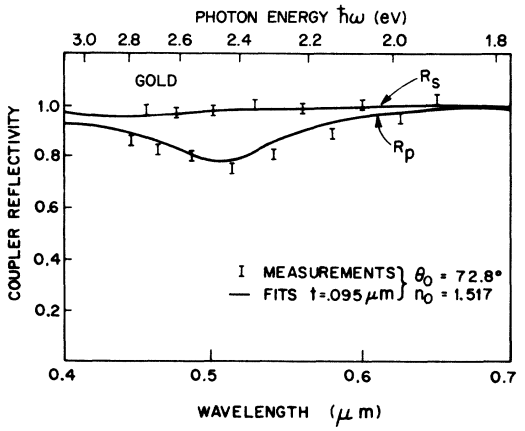

FIG. 4. Coupler reflectivity measured at D in Fig. 2 for two polarizations. The p-polarized beam couples with the surface plasmons and shown a prominent dip. The solid curves shown fits using the equations of Sec. II and the parameters in the figure.

reflection spectrum for a glass prism coupler under the condition $n_0 \sin\theta_0 = 1.45$. The p-polarized (R_p) and s-polarized (R_s) spectra are measured separately and separately normalized by removing the gold sample and repeating the run with only the prism in the beam. In fact, this procedure was found to lead to relatively large uncertainties because of the long term gain stability required. Once the basic form of surface-plasmon absorption was confirmed in Fig. 4, it was found better to measure the ratio R_p/R_s. This was accomplished by scanning through a spectral region with the polarizer set for p-polarization, immediately repeating the scan with the polarizer set for s polarization, and then dividing the data. These ratio spectra could then be corrected later by a ratio spectrum taken with no sample present. The no-sample spectrum is necessary to correct for the polarization characteristics of the instrument. Figures 5 and 6 show the plasmon spectra of gold samples taken by this latter method for $n_0 \sin\theta_0 = 1.45$ and for smaller $k_{\parallel}$ at $n_0 \sin\theta_0 = 1.1$.

To investigate the surface plasmon at larger wave vectors than shown in Figs. 4–6, Eq. (2) shows that a larger index is necessary. A strontium titanate 60°-60°-60° prism was prepared ($n_0 = 2.472$ at $\lambda = 0.5$ μm).[13] For optimum coupling the air gap must now be reduced [Eq. (4)] to observe the surface plasmon. To surmount the difficult mechanical problem of providing the small air gaps, a spacing layer of silica was evaporated onto the base of the prism and the gold then evaporated directly onto the silica. Three silica evaporations using a movable mask allowed three spacings to be studied during one run. Figure 7 shows the prism, silica layers, and gold with the layer thickness greatly exaggerated. Figures 7 and 8 show the experimental results R_p/R_s for four of the thicknesses measured.

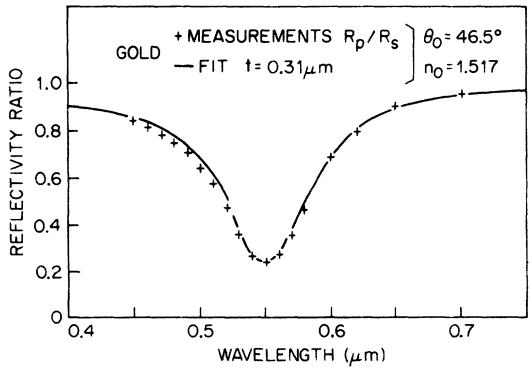

FIG. 5. Ratio spectrum showing the gold surface plasmon at smaller θ_0 (i.e., smaller $k_{\parallel}$ than Fig. 4). The mode has shifted to lower energy.

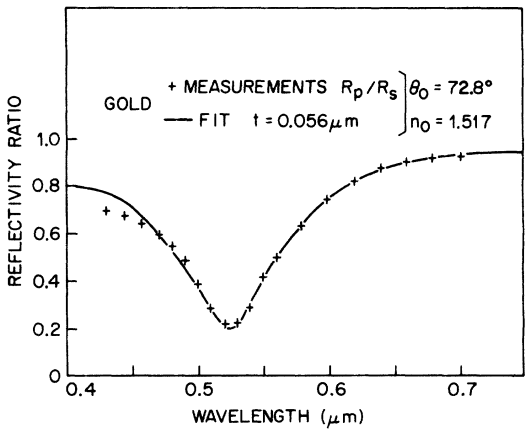

FIG. 6. Ratio spectrum showing gold surface plasmon under conditions similar to Fig. 4 but with stronger coupling.

III. RESULTS; SPECTRA AND FITS

A. Optical Constants of Gold

Before discussing the fits to the data presented above, we must consider the optical constants of bulk gold. In examining the data and the parameters used, we found no evidence that we were seeing any specific surface effects. Even though the surface plasmon has its maximum electric field and current density at the surface, there is an exponential tail for both these fields extending into the metal. For the range of $k_{\parallel}$ we have investigated, the exponential penetration $1/\mathrm{Re}q_2$ was always greater than 300 Å. For these experiments, therefore, the surface plasmons are controlled predominantly by the bulk dielectric properties.[14]

Beaglehole[15] and Thèye[16] have presented data on the imaginary part of the dielectric function ϵ'' of gold. We have used their data as starting values and then made small adjustments in the process of fitting the surface-plasmon absorption.[17] Figure 9 (solid curve) shows our results for both the real and the imaginary parts of the dielectric function $\epsilon = \epsilon' + i\epsilon''$. Our fits determine ϵ' and ϵ'' in the range 0.4–0.7-μm wavelength. In Fig. 9 the dielectric constant is shown in this range and extrapolated to somewhat shorter wavelengths using the parameters of the fit. The extrapolation is quite reliable since the data of Thèye show no major resonances at these short wavelengths. The surface-plasmon dip determines ϵ' and ϵ'' independently and quite accurately near the frequency where R_p is a minimum.[18] The R_p/R_s measurements represent a new way of obtaining optical constants for a medium (metal or dielectric), which can be very accurate in the region where ϵ' is negative. In the present study we have not concentrated on obtaining highly accurate values of $\epsilon' + i\epsilon''$ but rather on

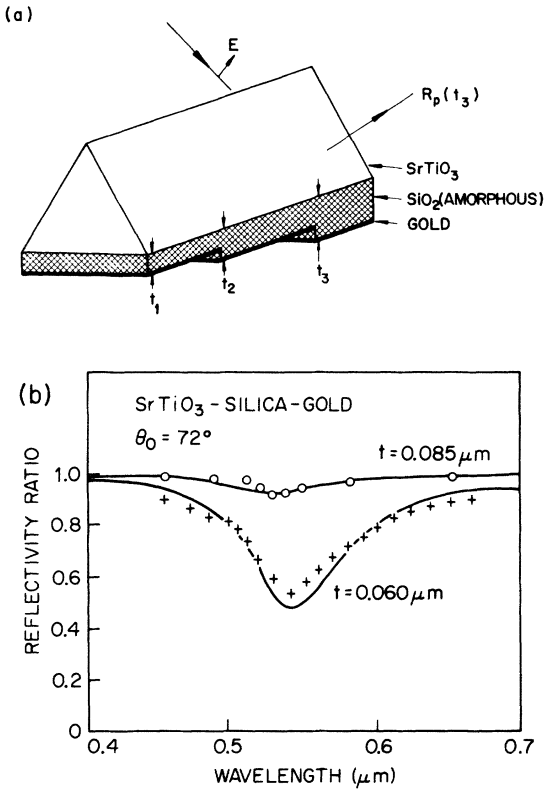

FIG. 7. (a) $SrTiO_3$ prism used to provide a large index for large-$k_{\parallel}$ spectra. A stepped silica layer provides three different spacings between the prism and gold sample. (b) Two ratio spectra showing the surface plasmon at the gold-silica interface.

measuring the surface plasmon and its dispersion. Thèye has shown that any accurate measurements of the dielectric properties of gold must be coupled with a study of the preparation conditions and with other physical properties of the evaporated film.[16]

If we use the approximate condition $\epsilon' = -1$ for the occurrence of large-wave-vector surface plasmons, then Fig. 9 shows that there will be a surface mode near 2.6 eV ($\lambda = 0.48$ μm). This point is labeled A. Another surface mode should occur near 3.1 eV (B) and a third near 4.5 eV (C).[19] ϵ'' is so large at these latter energies, however, that the approximate resonance condition is almost useless in analyzing the data. The experimental peaks can be expected to be broad and shifted away from these energies. The spectra presented below deal with the surface plasmon at A and its dispersion as a function of $k_{\parallel}$.

B. Fits to Surface-Plasmon Spectra

Figure 4 shows separate measurements of R_p and R_s using a glass prism and rather large air gap. The coupling to the surface plasmons is evident near $\lambda = 0.5$ μm. R_p has been calculated and good agreement is obtained for that polarization, which couples to the surface plasmons. No coupling occurs for R_s since the electric vector in the beam is orthogonal to the polarization fluctuations of the surface plasmons (Fig. 1). The R_s calculation shows only a very weak dip at the short-wavelength end of the spectrum, which is connected with the bulk plasmons. The thickness $t = 0.095$ μm used in the calculation is obtained by a best fit to the data. It is within 15% of that estimated for the air gap by observing Newton's rings. This agreement was felt to be satisfactory. θ_0 and n_0 are given in Fig. 4. Both are measured independently to a sufficient accuracy that the uncertainties in the experiments are controlled by detector noise and possibly by nonuniformity in the spacing t.

In Figs. 5 and 6 the data have been fit by calculating R_p/R_s. The fitting procedure consists of making small adjustments in $n_2 = \sqrt{\epsilon}$ and in t in Eqs. (5)–(10), then calculating a spectrum. The best-fit dielectric function of gold, considering all spectra together, has been presented in Sec. III A. The spacing t was found in each case to be within 30% of the value aimed for in laying down the metallic spacers or the silica layers. Comparison of Figs. 4 and 6 clearly shows the overcoupling effect—the surface-plasmon dip is pushed to larger wavelength when the prism is brought close to the gold.

It is appropriate here to consider the nature of the resonance shown in Figs. 4–6. At the lowest

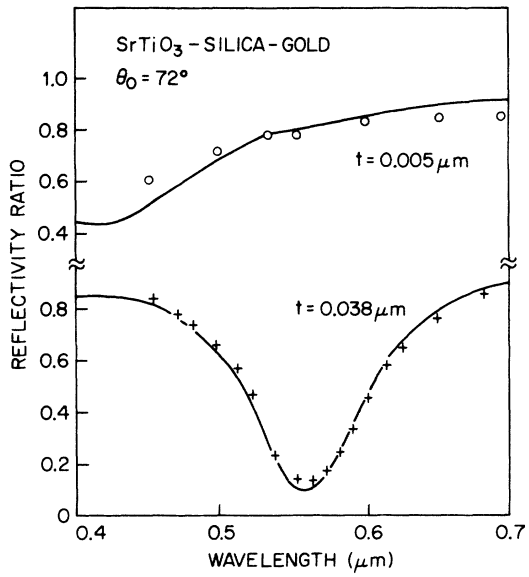

FIG. 8. Ratio spectra taken with extremely thin silica spacers. In the top part of the figure the large overcoupling has washed out the surface-plasmon dip but left some sign of the bulk-plasmon reflectivity edge near 0.5 μm.

energies shown in Fig. 9 the response is clearly of free-electron or Drude form.[20] If the resonance dip had occurred at these low energies, the oscillating polarization would be entirely composed of free-carrier motion and we could talk of the free-electron surface plasmon. In fact, at 2.36 eV the polarization response consists of two components almost 180° out of phase. Twenty-two percent of the total is bound d-electron response and 78% is free-electron response.[21] Therefore, the surface plasmon is partially a d-electron mode and, in fact, its width is predominantly controlled by ϵ'' of the d-electron transitions. From Fig. 9 it can be seen that if dips in R_p are measured near resonances B and more especially near C, they would be almost pure surface d-electron modes since in these regions the free-electron response has dropped to a small fraction of the total response. Figure 10 shows the predicted form of these higher resonances using a glass prism coupler; however, no experimental scans were made because of the limited spectral range of the equipment.

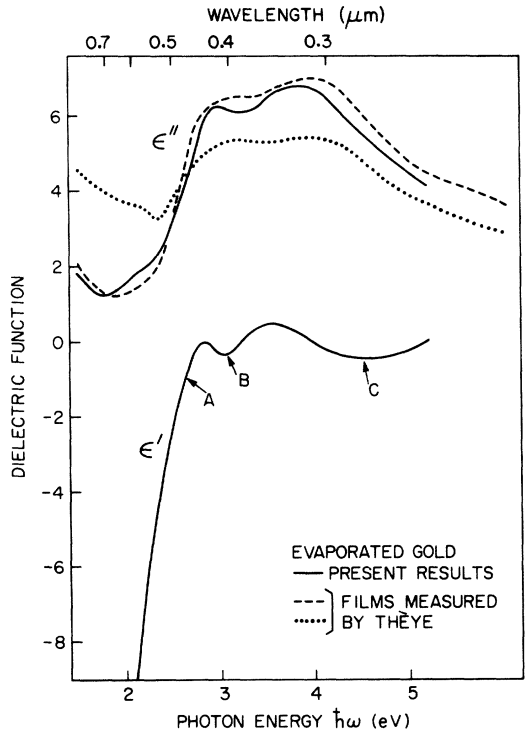

FIG. 9. Dielectric function of gold. The dashed curve is the imaginary part ϵ'' for a well-annealed sample prepared by Thèye. We used this curve as a starting point in the fits. The solid curve is the resultant best fit to all our surface-plasmon dips. The lower part of the figure shows the corresponding real part of ϵ. The frequencies labeled A, B, and C are potential surface-plasmon modes for a gold-air interface since ϵ is passing through -1 at complex frequencies near these positions.

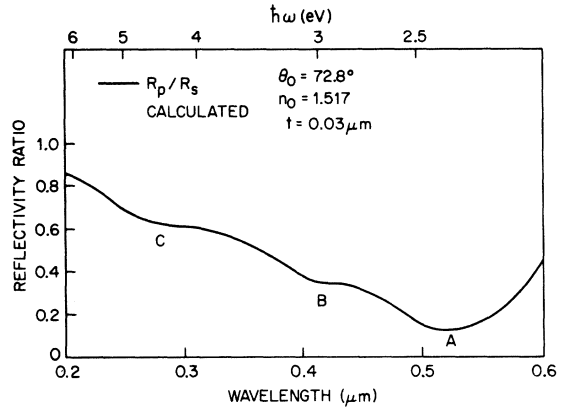

FIG. 10. Calculated prism coupler reflectivity at short wavelength showing all three surface plasmons of Fig. 9. The two short-wavelength resonances result almost entirely from the d-electron transitions and are weak because ϵ'' is large in this region.

IV. RESULTS; DISPERSION AND RANGE

A. Dispersion of Surface Plasmons

Equation (2) shows that the surface-plasmon reflection dip may be studied for different values of surface wave vector $k_{\parallel}$. This is done by choosing different values of $n_0 \sin\theta_0$ for each scan. The result when suitably plotted gives the surface-plasmon dispersion curve. Figure 11 shows the measured dispersion for the mostly-free-electron-like surface mode in gold (mode A in Fig. 9). The dashed lines are the ω-vs-$k_{\parallel}$ locus of Eq. (2). Note that if we had continuously varied θ_0 during a frequency scan to obey

$$\theta_0 = \sin^{-1}(ck_{\parallel}/n_0\omega)\,, \tag{11}$$

we could have obtained constant-$k_{\parallel}$ scans. Such scans would be quite useful at small $k_{\parallel}$, where the scan locus becomes almost tangent to the dispersion curve.

The solid points shown in Fig. 11 mark the position of the minimum of R_p/R_s in the limit of large t. In each case R_s is nearly constant, so that no significant error arises from using the minimum of R_p itself. At smaller t, coupling effects push the observed minimum to a different frequency. The dashed curve farthest to the right shows the ω-$k_{\parallel}$ scan that is obtained for the $SrTiO_3$ prism. In fact, no usable data were obtained for the gold-air-$SrTiO_3$ system because of the extreme sensitivity of the data to variations in the very small value of t. As mentioned previously, measurements were performed in the gold-silica-$SrTiO_3$ system. The dispersion curve measured for this system is for the gold-silica interface plasmon. Figure 11 shows this point; it falls at considerably lower en-

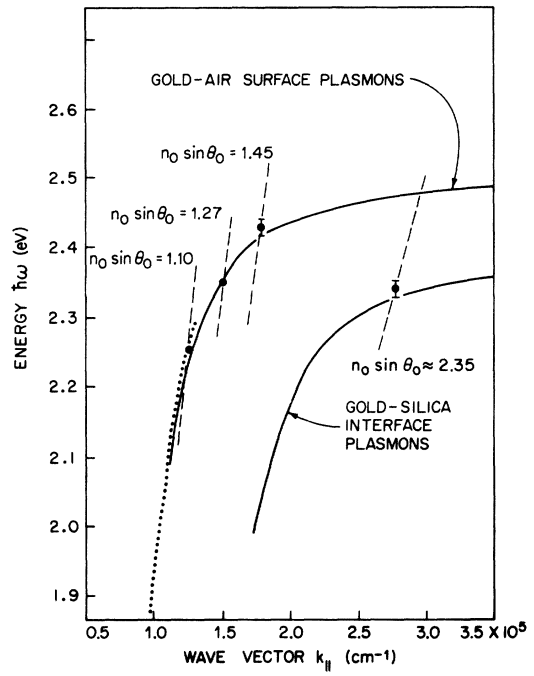

FIG. 11. Surface-plasmon dispersion curve. The solid curve is calculated and agrees quite well with the measured points. As indicated in the text, the point near $k_{\parallel} = 3\times10^5$ cm^{-1} could not be measured on the gold-air curve because of the very small air gap required. The corresponding point could be measured with a silica spacer giving one point on the lower (gold-silica) plasmon curve. The dotted curve shows the measured results of Ritchie *et al.* using a gold grating. The dispersion curves associated with modes B and C of Fig. 9 have not been measured and their calculated positions are omitted for clarity.

ergy than the gold-air dispersion curve.

The solid curves in Fig. 11 are the calculated dispersion curves appropriate to the measurements performed here. They are the locus of minima in R_p/R_s calculated using our "best-fit" dielectric function for gold. Other dispersion curves could be constructed based on other response functions. In earlier work it was proposed[8] that the locus of peaks in the imaginary part of the response function $T(k_{\parallel}, \omega)$ be used for comparison with experiment. This method gives a good comparison with the measured reflectance dips for some cases studied earlier.[8] The damping is so large for the present case that such a dispersion curve lies at much higher energy than the solid curves of Fig. 11. Overall, there is good agreement between theory and experiment for the dispersion curves based on the reflection minima.

The dotted curve in Fig. 11 shows the dispersion of surface plasmons in gold measured by Ritchie *et al.* using the technique of scattering from a gold grating.[11] This method appears to work best in the low-energy region where the surface excitation is mostly photonlike. The methods are thus complementary. The small discrepancy between the dispersion curves where they overlap would be removed if we had reduced our reflectivity data to T, the surface-charge response function, and plotted peaks in ImT for both theory and experiment. That is, the discrepancy is probably real, but trivial, in that it results from measuring different response functions related to the same excitation.

B. Range of Surface Plasmons

The surface plasmon takes on more photonlike character at small $k_{\parallel}$. Here, it is more properly called a surface polariton. In this small-$k_{\parallel}$ region it acquires a range of many times $1/k_{\parallel}$ and may emerge from under the coupling prism and travel some distance along the gold-air interface. At much lower frequencies this surface mode is just the surface guided wave familiar in radio and microwave engineering. Schoenwald *et al.* have measured the range of surface plasmons on copper using the 10-μm laser and two coupling prisms.[22] They find a range at this wavelength of about 0.3 cm. While we have performed no direct range measurement, the range information is implicit in the analysis already carried out.

In the Appendix we show that the range is given by

$$L = 0.5/\mathrm{Im}\left[\frac{\omega}{c}\left(\frac{\epsilon}{\epsilon+1}\right)^{1/2}\right]. \tag{12}$$

This is a general result, good at any frequency for a surface wave at an interface between a medium characterized by $\epsilon(\omega)$ and vacuum (or air). Figure 12 shows the calculated range for gold as a function of the frequency of the driving field. At the highest frequencies shown the range is about 0.4 μm and shows structure associated with the d-band transitions. At lower frequencies the range increases rapidly and approaches an ω^{-2} dependence due to the dominance of the Drude term we have used for the free-carrier part of $\epsilon(\omega)$. For $\omega \ll \omega_n$ the Drude term

$$\epsilon_D = \omega_n^2/(-\omega^2 - i\omega\Gamma) \tag{13}$$

dominates the dielectric function. The parameter $\omega_n = 73500$ cm^{-1} and the collision frequency $\Gamma = 550$ cm^{-1} have been determined from our fits described previously. In constructing Fig. 12 we have extrapolated Eq. (13) to frequencies where the Γ value given above may not be valid and is probably lower.[23]

The straight line portion of Fig. 12 will be universally valid for any metal with Drude-type behavior. In this region of $\omega \ll \omega_n$ the range simplifies to

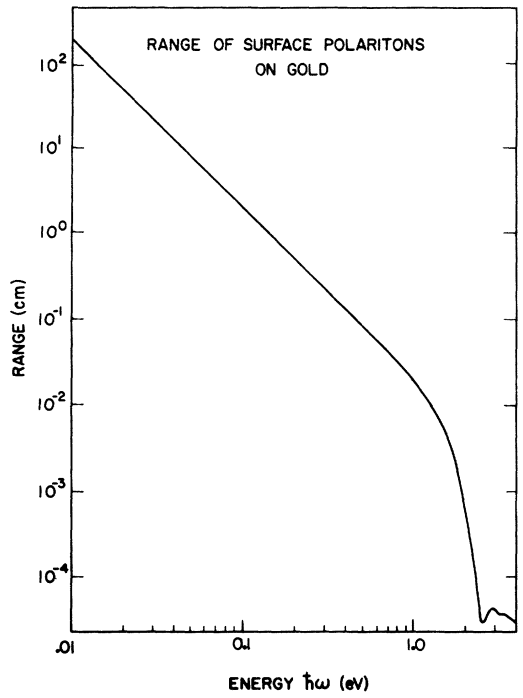

FIG. 12. Range of surface polaritons at a gold-air interface. These results are calculated using the dielectric function of gold presented earlier. The dc conductivity of gold suggests that a smaller Γ should be used at low frequencies which would result in larger ranges than shown at the left-hand side of the figure.

$$L \approx c\omega_p^2/\omega^2\Gamma\,, \tag{14}$$

Equation (14) illustrates an inverse dependence on the scattering frequency Γ and also the ω^{-2} dependence mentioned earlier.

ACKNOWLEDGMENTS

It is a pleasure to acknowledge the help of F. K. Reinhart and J. J. Schott in preparing the silica layers and of W. L. Feldmann for the gold evaporations. The author wishes to thank D. A. Kleinman for several valuable discussions of the range integral. The capable assistance of J. A. Ditzenberger in making the optical measurements is greatfully acknowledged.

APPENDIX: RANGE OF SURFACE POLARITONS

Table I shows the surface-polariton response to an applied surface change of arbitrary (complex) surface wave vector and frequency. We evaluate the range now by two methods. First, consider a surface-polariton wave proceeding to the right of $x=0$ (Fig. 1). For $x>0$ no drive is provided so that

$$\rho_{ext}=0, \quad x>0\,. \tag{A1}$$

To sustain the wave some device is needed for $x<0$ to provide suitable normal and tangential components of field in the proper phase relationship. The time dependence of the driving source is chosen to be of the form $e^{-i\omega t}$ with ω real. Such a source device is more complicated than a prism coupler; however, its actual realization is of no importance here. For there to be nonzero fields such as $E_2^{\perp}$ present, Eq. (A1), combined with the results in Table I, shows that we must have $T\equiv\infty$. Squaring and rearranging the denominator of T, we find that k must satisfy the equation:

$$k=k_0\equiv\frac{\omega}{c}\left(\frac{\epsilon}{\epsilon+1}\right)^{1/2}\,. \tag{A2}$$

Since the electric field was postulated to propagate as e^{ikx}, the right-hand side of Eq. (A2) is evaluated for real frequency and the imaginary part separated out. The power carried by the fields will fall to $1/e$ in the distance L (the range) where

$$L=\frac{0.5}{\mathrm{Im}k_0}=0.5\Big/\mathrm{Im}\left[\frac{\omega}{c}\left(\frac{\epsilon}{\epsilon+1}\right)^{1/2}\right]\,. \tag{A3}$$

Equation (A3) may be directly evaluated once $\epsilon(\omega)$ is known.

The second method of finding the range uses the response function in more detail. In this method we actually specify the source distribution and look for waves proceeding from the source. Consider the source

$$\rho_{ext}(x,z,t)=Q\delta(z)\delta(x)e^{-i\omega t}\,. \tag{A4}$$

We are using the coordinate system of Fig. 1. Equation (A4) represents an oscillating line of charge infinitely extended in the y direction. We take ω to be real and look for the response of the system to the right of $x=0$. Since the response function T gives the response for any source distribution, we merely use superposition to obtain the response for the source given by Eq. (A4). The δ-function source has the k-space spectrum $1/(2\pi)^{1/2}$, that is,

$$\delta(x)=\frac{1}{(2\pi)^{1/2}}\int_{-\infty}^{\infty}\frac{e^{ikx}}{(2\pi)^{1/2}}\,dk\,.$$

The contour along the real k axis can be closed in the upper half-plane when we consider $x>0$. Integrating this source spectrum along with the response function T, we obtain for the normal electric field component

$$E_2^{\perp}(x>0,z=0)=c_1\int_{-\infty}^{\infty}\frac{e^{ikx}\,dk}{-\epsilon-(1-\epsilon\omega^2/c^2k^2)^{1/2}/(1-\omega^2/c^2k^2)^{1/2}}\,, \tag{A5}$$

where c_1 absorbs simple constants. The integral has a pole and a branch cut in the upper half-plane. It is trivial to establish that the pole is first order and is at the location given by Eq. (A2). Using the method of residues, the pole at k_0 [Eq. (A2)] gives a field whose spatial dependence is

$$E_2^{\perp}(x>0,\ z=0)=c_2 e^{ik_0 x}\ , \tag{A6}$$

so that this pole contribution gives waves of the same form and range as given in Eq. (A3). This equation was used together with the gold data to construct Fig. 12.

The branch-cut contribution to the integral is more difficult to evaluate. The cut (and hence the branch-cut integral) extends from $k^2=\omega^2/c^2$ to $k^2=\epsilon\omega^2/c^2$. Two approximations may be used to derive an analytic form. Restricting ourselves to the region where $|\epsilon| \gg 1$ allows the upper end of the cut to be moved to infinity. Physically the restriction puts us in the Drude region described earlier. Secondly, we examine only the far field pattern; i.e., x is chosen large enough so that the factor e^{ikx} in Eq. (A5) causes the small-k region to dominate. Using these approximations Eq. (A5) gives (for $x \gg 0,\ \omega > 0$)

$$E_2^{\perp}(x\gg 0,\ z=0)=\frac{c_3\omega^{1/2}e^{i\omega x/c}}{|\epsilon|^{3/2}x^{1/2}}\ . \tag{A7}$$

The exponential factor shows this to be a wave traveling to the right with only weak attenuation from the $x^{-1/2}$ factor. This latter factor suggests that our particular source has set up a cylindrical wave traveling above the surface. Since the wave has a power-law falloff, we don't define a range for this branch-cut term. The analysis suggests that this wave may be present in sharply restricted sources (such as right-angled prisms) and should be discriminated against in making range measurements for the true surface wave.

[1] D. Pines, *Elementary Excitations in Solids* (Benjamin, New York, 1963).

[2] R. H. Ritchie, Phys. Rev. **106**, 874 (1957).

[3] E. A. Stern and R. A. Farrell, Phys. Rev. 120, 130 (1960).

[4] C. Kunz, Z. Phys. **196**, 311 (1966).

[5] A. Otto, Z. Phys. **216**, 398 (1968).

[6] It should be noted that the conventional ATR method is used in regions of very-weak absorption where the evanescent field of the prism penetrates the sample even with zero air gap between them. See, for example, N. J. Harrick, *Internal Reflection Spectroscopy* (Interscience, New York, 1967).

[7] N. Marschall and B. Fischer, Phys. Rev. Lett. **28**, 811 (1972).

[8] A. S. Barker, Jr., Phys. Rev. Lett. **28**, 892 (1972).

[9] V. V. Bryksin, Yu M. Gerbshtein and D. N. Mirlin, Fiz. Tverd. Tela **14**, 543 (1972) [Sov. Phys.-Solid State **14**, 453 (1972)].

[10] A. S. Barker, Jr., Surf. Sci. **34**, 62 (1973).

[11] R. H. Ritchie, E. T. Arakawa, J. J. Cowan, and R. N. Hamm, Phys. Rev. Lett. **21**, 1530 (1968).

[12] O. S. Heavens, *Optical Properties of Thin Solid Films* (Academic, New York, 1955), Chap. 4.

[13] W. Bond, J. Appl. Phys. **36**, 1674 (1965).

[14] P. J. Feibelman, [Phys. Rev. Lett. **30**, 975 (1973)] has evaluated correction terms to the surface plasmon energy due to the shape of the potential barrier at a metal surface. Even at the largest values of $k_{\parallel}$ which we have measured, these specific surface effects shift the plasmon frequency less than 0.3% downwards.

[15] D. Beaglehole and E. Erlbach, Solid State Commun. 8, 255 (1970).

[16] Marie-Luce Thèye, Phys. Rev. B **2**, 3060 (1970).

[17] H. W. Verleur, J. Opt. Soc. Am. **58**, 1356 (1968).

[18] Since the gold films used in the present experiments were not carefully prepared to minimize impurities and structural defects, Fig. 9 must be regarded as giving the optical constants of these particular films. See Ref. 16 for a more complete discussion of the relation of ϵ to the structural properties of gold films.

[19] Figure 9 is drawn for real frequencies. The dispersion wiggles at B and C predict that a solution to $\epsilon = -1$ can be found for frequencies off the real-frequency axis in the complex-frequency plane.

[20] H. E. Bennett and J. M. Bennett, in *Optical Properties and Electronic Structure of Metals and Alloys*, edited by F. Abelis (North-Holland, Amsterdam, 1966) p. 175.

[21] These figures are obtained by examining the dielectric constant $\epsilon(\omega)$ at 2.36 eV. Since the fit to ϵ (Ref. 17) has separate free-electron and bound (d-electron) terms, the magnitude and phase of the polarization corresponding to each term is easily evaluated at any frequency.

[22] J. Schoenwald, E. Burstein, and J. M. Elson, Solid State Commun. **12**, 185 (1973).

[23] The dc conductivity of well-annealed thick gold films at 300 K requires $\Gamma = 220\ \text{cm}^{-1}$.